ELSEVIER

Computational Materials Science 16 (1999) 2–9

COMPUTATIONAL MATERIALS SCIENCE

Simulation of texture induced elastic anisotropy of polycrystalline copper

A. Bertram *, T. Böhlke

Institüt für Mechanik, Otto-von-Guericke-Universität, Universitatsplatz 2, 39106 Magdeburg, Germany

Abstract

The texture induced elastic anisotropy of polycrystalline copper is studied for different finite deformation paths. As a homogenization technique, the Taylor–Lin model is used, which is a first-order theory and incorporates only a volume-fraction representation of microstructure. In order to identify the anisotropy of the macroscopic elastic behaviour, approximations of the macroscopic strain energy density corresponding to different symmetry groups are determined and compared.

Keywords: Finite inelasticity; Induced anisotropy; Texture development

1. Introduction

Since single crystalline copper exhibits a significant degree of elastic anisotropy, the polycrystalline elastic properties can be affected by the crystallographic texture in an amount that can be relevant for engineering applications [8,17,23]. The crystallographic texture evolution of materials with high and intermediate stacking fault energy (e.g., pure copper) can be determined by the Taylor–Lin model within a first-order accuracy [16]. In the present paper the evolution of the elastic properties of polycrystalline copper undergoing large inelastic deformations is numerically studied for three finite deformation modes using the Taylor–Lin model [2].

The elastic law on the microscale, i.e., within the grains, is derived from the assumption that elastic ranges exist and the corresponding elastic behaviour is not affected by inelastic deformations [3]. The simulations are concentrated on deformation processeses with a constant velocity gradient. Therefore, only isotropic hardening models [13,19] are applied. The hardening parameters are taken from the literature [24].

For a given texture there are different methods to determine the corresponding elastic properties of the aggregate [15]. Simple estimations are those suggested by Voigt [22] and Reuss [21]. The advantage of these approaches is that they represent upper and lower bounds for the strain energy of the real material [14,20]. The disadvantage of them is that the distance between the bounds increases with the anisotropy of the elastic behaviour in the grains.

Alternative approaches have been developed in order to obtain more precise information from the texture data. Hill [14] proposed both an arithmetic

* Corresponding author.
E-mail address: bertram@mb.uni-magdeburg.de (A. Bertram).

0927-0256/99/$ - see front matter
PII: S0927-0256(99)00039-7

and a geometric mean of the isotropic bounds by Voigt and Reuss, which give estimations closer to experimental values. An approach that focusses on a homogenization that guarantees unique effective properties, was given by Aleksandrov and Aizenberg [1] and further developed by Matthies and Humbert [18]. Within that approach the geometric mean of the local elastic moduli is used. Beside the uniqueness, the advantage of this method lies in improved predictions of experimental values.

Some knowledge concerning the symmetry of the macroscopic elastic behaviour is helpful for the development of phenomenological models describing deformation induced anisotropy. On the macroscopic scale non-triclinic material symmetries determined by experiments or simulations exist only in an approximate sense, because the microstructure induces deviations from the behaviour described by the classical point-groups. Since the elastic behaviour of metals can be linearized within the elastic ranges, a fourth-order tensor is sufficient for the description of the mechanical properties within all elastic ranges. In order to identify the anisotropy, the fourth-order elasticity tensor given by any homogenization technique can be approximated by fourth-order tensors corresponding to distinct symmetry groups. If an approximation is sufficient within a prescribed tolerance, the anisotropy can be considered as identified. In this paper an approximation is suggested, which contains the isotropic bounds as special cases if applied to the anisotropic bounds by Voigt and Reuss.

Notation: Throughout the text a direct tensor notation is used. In order to avoid additional formal definitions, the index notation is applied in some cases using the summation convention. Vectors and second-order tensors are denoted by small and capital bold Latin letters, respectively. Third- and fourth-order tensors are denoted by small bold Greek and capital bold Sans Serif letters. Linear mappings of second-order tensors are written as $\boldsymbol{A} = \mathsf{K}[\boldsymbol{B}]$. The scalar product, the dyadic product, and the Frobenius norm are denoted by, $\boldsymbol{A} \cdot \boldsymbol{B}$, $\boldsymbol{A} \otimes \boldsymbol{B}$, and $\|\boldsymbol{A}\| := (\boldsymbol{A} \cdot \boldsymbol{A})^{1/2}$, respectively. *Psym*, *Orth* and *Inv* represent the sets of symmetric and positive-definite, proper orthogonal and invertible second-order tensors.

2. Microscopic elastic behaviour

Elastic law: The reduced form $\boldsymbol{S} = \boldsymbol{h}_p(\boldsymbol{C})$ is used for the description of the single crystalline elastic behaviour, $\boldsymbol{S} := \boldsymbol{F}^{-1}\boldsymbol{T}\boldsymbol{F}^{-\mathrm{T}}$ being the material stress tensor, $\boldsymbol{F}$ the deformation gradient, $\boldsymbol{T}$ the Cauchy stress tensor and $\boldsymbol{C} = \boldsymbol{F}^{\mathrm{T}}\boldsymbol{F}$ the right Cauchy–Green tensor. The index p indicates the dependence of the function $\boldsymbol{h}$ on the current elastic range. In order to specify this dependence, it is assumed that the elastic behaviour on the microscale is not affected by inelastic deformations. This assumption is equivalent to the following statement. Let $\boldsymbol{h}_p$ and $\boldsymbol{h}_0$ be two elastic laws of the same material point corresponding to elastic ranges before and after an inelastic deformation, then $\boldsymbol{h}_p$ and $\boldsymbol{h}_0$ are isomorphic, i.e., there exists a material isomorphism $\boldsymbol{P} \in \mathit{Inv}$ such that

$$\boldsymbol{h}_p(\boldsymbol{C}) = \boldsymbol{P}\boldsymbol{h}_0(\boldsymbol{P}^{\mathrm{T}}\boldsymbol{C}\boldsymbol{P})\boldsymbol{P}^{\mathrm{T}} \tag{1}$$

holds for all $\boldsymbol{C} \in \mathit{Psym}$ [3,4,6]. As a result, the current elastic law can be represented by a referential elastic law $\boldsymbol{h}_0$ and an invertible second-order tensor $\boldsymbol{P}$, called plastic transformation. Within the elastic ranges of metals, physically linear laws are sufficient for the description of elasticity. If the linearization is carried out with respect to the referential law $\boldsymbol{h}_0$, one obtains

$$\boldsymbol{S} = \boldsymbol{P}\mathsf{K}\left[\tfrac{1}{2}(\boldsymbol{P}^{\mathrm{T}}\boldsymbol{C}\boldsymbol{P} - \boldsymbol{I})\right]\boldsymbol{P}^{\mathrm{T}}. \tag{2}$$

The fourth-order stiffness tensor K and the corresponding compliance tensor M are specified by the symmetry group S of the material, being a subgroup of the orthogonal group, e.g., in terms of stiffnesses

$$\boldsymbol{H}^{\mathrm{T}}\mathsf{K}[\cdot]\boldsymbol{H} = \mathsf{K}\left[\boldsymbol{H}^{\mathrm{T}} \cdot \boldsymbol{H}\right] \quad \forall \boldsymbol{H} \in S \subseteq \mathit{Orth}. \tag{3}$$

For hyperelastic materials the elasticity tensors possess the major symmetry. Without loss of generality, the symmetry in its first and last pair of indices is assumed. Because of the cubic symmetry of the material under consideration, there exist the following projector representations [5]:

$$\mathsf{K} = \sum_{\alpha=1}^{3} \lambda_\alpha \mathsf{P}_\alpha, \qquad \mathsf{M} = \sum_{\alpha=1}^{3} \frac{1}{\lambda_\alpha}\mathsf{P}_\alpha \tag{4}$$

with $\mathbf{P}_1 = \frac{1}{3} I \otimes I$, $\mathbf{P}_2 = \mathbf{A} - \mathbf{P}_1$, $\mathbf{P}_3 = \mathbf{I}^S - \mathbf{P}_2$. I denotes the second-order identity tensor and $\mathbf{I}^S$ the symmetric part of the fourth-order identity tensor. The tensor $\mathbf{A}$ is given by the lattice vectors $\boldsymbol{g}_i$ as $\mathbf{A} = \sum_{i=1}^{3} \boldsymbol{g}_i \otimes \boldsymbol{g}_i \otimes \boldsymbol{g}_i \otimes \boldsymbol{g}_i$. The projectors $\mathbf{P}_\alpha$ are idempotent $\mathbf{P}_\alpha \mathbf{P}_\alpha = \mathbf{P}_\alpha$, biorthogonal $\mathbf{P}_\alpha \mathbf{P}_\beta = \mathbf{0}$ $(\alpha \neq \beta)$, and complete $\sum_{\alpha=1}^{3} \mathbf{P}_\alpha = \mathbf{I}^S$. The eigenvalues or Kelvin moduli λ_α of the stiffness tensor can be expressed by its components with respect to a Cartesian coordinate system that coincides with the symmetry axes of the material in the following form: $\lambda_1 = K_{1111} + 2K_{1122}$, $\lambda_2 = K_{1111} - K_{1122}$, $\lambda_3 = 2K_{1212}$. In the case of isotropy, the elastic law is determined by two projectors $\mathbf{P}_1^I = \mathbf{P}_1$, $\mathbf{P}_2^I = \mathbf{I}^S - \mathbf{P}_1^I$, and the corresponding eigenvalues by $\lambda_1 = K_{1111} + 2K_{1122}$, $\lambda_2 = K_{1111} - K_{1122} = 2K_{1212}$.

3. Macroscopic elastic behavior

Bounds for the stored energy: Voigt's and Reuss' assumption of constant strain and stress fields, respectively, yield the most simple estimation of the elastic properties of the aggregate. The macroscopic elasticity tensors are then given as volume averages of the corresponding local fields, and imply upper and lower bounds for the macroscopic strain energy density [14,20]:

$$\mathbf{K}^V = \frac{1}{V} \int_V \mathbf{K} \, \mathrm{d}V, \quad \mathbf{M}^R = \frac{1}{V} \int_V \mathbf{M} \, \mathrm{d}V. \tag{5}$$

Note that $\mathbf{K}^{V-1}$ and $\mathbf{M}^R$ are distinct in general. In general, these volume averages are triclinic if applied to empirical texture data. An estimation of the properties with the additional assumption of uniformly distributed grain orientations follows by transforming the integrals (5) to the orientation space g and setting the orientation distribution function f constant [8]. If the orientation space is parameterized by Euler angles, one obtains with $\mathrm{d}V/V = f \, \mathrm{d}g = \sin(\Phi) \, \mathrm{d}\Phi \, \mathrm{d}\varphi_1 \, \mathrm{d}\varphi_2 / 8\pi^2$,

$$\begin{aligned} \mathbf{K}^{VI} &= \int_g \mathbf{K} \frac{\sin(\Phi)}{8\pi^2} \, \mathrm{d}\Phi \, \mathrm{d}\varphi_1 \, \mathrm{d}\varphi_2, \\ \mathbf{M}^{RI} &= \int_g \mathbf{M} \frac{\sin(\Phi)}{8\pi^2} \, \mathrm{d}\Phi \, \mathrm{d}\varphi_1 \, \mathrm{d}\varphi_2. \end{aligned} \tag{6}$$

The integration yields the well-known isotropic elasticity tensors, which imply bounds for the isotropic behaviour [14,21,22]. The corresponding eigenvalues are given by

$$\begin{aligned} \lambda_1^{VI} &= \tfrac{1}{3} K_{iijj}, \quad \lambda_1^{RI^{-1}} = \tfrac{1}{3} M_{iijj}, \\ \lambda_2^{VI} &= \tfrac{1}{15}(3K_{ijji} - K_{iijj}), \quad \lambda_2^{RI^{-1}} = \tfrac{1}{15}(3M_{ijji} - M_{iijj}). \end{aligned} \tag{7}$$

The distance between the upper and lower bound depends on the degree of elastic anisotropy. In the case of aggregates of cubic single crystals the distance can be expressed in terms of the Zener anisotropy ratio Z by

$$\frac{\|\mathbf{K}^{VI} - \mathbf{K}^{RI}\|}{K_{1111} - K_{1122}} = \frac{6\sqrt{5}(Z-1)^2}{5(2Z+3)}, \quad Z := \frac{2K_{1212}}{K_{1111} - K_{1122}}. \tag{8}$$

Isotropy condition: The tensors $\mathbf{K}^V$ and $\mathbf{M}^R$ can be decomposed into their isotropic and anisotropic parts:

$$\begin{aligned} \mathbf{K}^V &= \mathbf{K}^{VI} + \|\mathbf{K} - \mathbf{K}^{VI}\| \mathbf{D}, \\ \mathbf{M}^R &= \mathbf{M}^{RI} + \|\mathbf{M} - \mathbf{M}^{RI}\| \mathbf{D}. \end{aligned} \tag{9}$$

For uniform polycrystals consisting of cubic single crystals, the tensor $\mathbf{D}$ depends only on the orientation distribution in the aggregate and is given by

$$\mathbf{D} = \frac{\sqrt{30}}{30} \left(I \otimes I + 2\mathbf{I}^S - \frac{5}{V} \int_V \mathbf{A} \, \mathrm{d}V \right). \tag{10}$$

This result follows from Eqs. (4), (5) and (7). According to Eqs. (9) and (10), the distance between the averages, e.g., $\mathbf{K}^V$ and $\mathbf{K}^{VI}$, is influenced on the one hand by the degree of anisotropy of the single crystals through

$$\|\mathbf{K} - \mathbf{K}^{VI}\| = \frac{\sqrt{30}}{5} (2K_{1212} - (K_{1111} - K_{1122})), \tag{11}$$

and on the other hand by the orientation distribution in form of the tensor $\mathbf{D}$. This representation implies an isotropy condition, i.e., $\mathbf{D} = \mathbf{0}$, in terms of crystal orientations for both the Voigt and the Reuss bound. With the proper orthogonal tensor $Q = \boldsymbol{g}_i \otimes \boldsymbol{e}_i$ one obtains an equivalent formulation of the isotropy condition,

$$\frac{1}{V}\int_V \sum_{k=1}^{3} Q_{ik}Q_{jk}Q_{mk}Q_{nk}\,\mathrm{d}V = \tfrac{1}{5}\left(\delta_{ij}\delta_{mn}+\delta_{im}\delta_{jn}+\delta_{in}\delta_{jm}\right). \tag{12}$$

The right-hand side of Eq. (12) represents a special case of the general isotropic fourth-order tensor. The norm $\|\mathbf{D}\|$ is equal to one only for a single orientation, equal to zero only for a uniform orientation distribution, and in between $(0, 1)$ otherwise. Since $\|\mathbf{D}\|$ is dimensionless, it can be interpreted as a scalar measure for the elastic anisotropy. For the case of piecewise constant orientations in the aggregate, exact solutions of Eq. (12) were found by Gaffke and Heiligers [10]. Since for these solutions both the Voigt and the Reuss average are exactly isotropic, their arithmetic mean as suggested by Hill [14] is isotropic as well. Furthermore, it can be shown that the geometric mean results in isotropic effective properties if $\mathbf{D} = \mathbf{0}$ holds.

The deviation from the isotropic elastic state of the aggregate can be expressed in terms of stiffnesses and compliances using the tensor $\mathbf{D}$. Starting from Eq. (9), one obtains the following material dependent estimations:

$$\frac{\|\mathbf{K}^V-\mathbf{K}^{VI}\|}{\|\mathbf{K}^{VI}\|} = f^V\|\mathbf{D}\|, \quad \frac{\|\mathbf{M}^R-\mathbf{M}^{RI}\|}{\|\mathbf{M}^{RI}\|} = f^R\|\mathbf{D}\|. \tag{13}$$

As examples for both a weakly and a strongly anisotropic material, the coefficients for aluminium and copper are given: $f^V_{\mathrm{Al}} = 0.043$, $f^R_{\mathrm{Al}} = 0.098$, $f^V_{\mathrm{Cu}} = 0.237$, $f^R_{\mathrm{Cu}} = 0.570$. The different magnitudes of f_{Al} and f_{Cu} explain that aluminium compared to copper exhibits for the same texture a much less pronounced elastic anisotropy.

Identification of material symmetry: According to Eq. (13) the differences between the triclinic and the isotropic bounds allow to quantify the degree of anisotropy of the aggregate. But so far no specific information concerning the symmetry of the aggregate is obtained. Since on the macroscopic scale material symmetries of the elastic behaviour generally exist only in some approximate sense, one faces the problem to identify non-triclinic and non-isotropic approximations, which can be qualified by an appropriate distance from the triclinic approximations.

In what follows, the approximation $\mathbf{K}^{VA}$ of the elasticity tensor $\mathbf{K}^V$ is determined by the condition that $\mathbf{K}^{VA}$ has the symmetry group S^A and minimizes the Frobenius norm of $\Delta\mathbf{K} := \mathbf{K}^V - \mathbf{K}^{VA}$. If there is an exact solution of equation $\|\Delta\mathbf{K}\| = 0$, the identification problem is equivalent to that posed and solved in [9].

As an example, it is shown that the isotropic bounds (6) solve the minimum problems $\|\mathbf{K}^V - \mathbf{K}^I\| \to \min$ and $\|\mathbf{M}^V - \mathbf{M}^I\| \to \min$, respectively, with $\mathbf{K}^I$ and $\mathbf{M}^I$ being isotropic fourth-order tensors. This result is straight-forward if the above mentioned projector representation of an isotropic elastic law is used, e.g., in terms of stiffnesses $\|\mathbf{K}^V - \lambda_1\mathbf{P}^I_1 - \lambda_2\mathbf{P}^I_2\| \to \min$. After setting the derivatives with respect to λ_1 and λ_2 equal to zero, one obtains equivalent to Eq. (7) $\lambda_1 = \mathbf{K}^V\cdot\mathbf{P}^I_1 \equiv \mathbf{K}\cdot\mathbf{P}^I_1 \equiv \lambda^{VI}_1$, and $\lambda_2 = \frac{1}{5}\mathbf{K}^V\cdot\mathbf{P}^I_2 \equiv \frac{1}{5}\mathbf{K}\cdot\mathbf{P}^I_2 \equiv \lambda^{VI}_2$.

4. Numerical example

Flow rule: Plastic deformations in single crystals at room temperature are dominated by slip mechanisms on specific crystallographic planes. For the description of copper a slip system theory with the twelve octahedral slip systems is applicable. The plastic transformation $\boldsymbol{P}$ is determined by the flow rule, which is specified by the slip system geometry, i.e., slip directions $\boldsymbol{d}_\alpha$, slip plane normals $\boldsymbol{n}^\alpha$, and corresponding slip system shearing rates $\dot{\mu}_\alpha$: $\dot{\boldsymbol{P}}\boldsymbol{P}^{-1} = -\sum_\alpha \dot{\mu}_\alpha \boldsymbol{d}_\alpha \otimes \boldsymbol{n}^\alpha$ [4]. The rates $\dot{\mu}_\alpha$ are functions of both the resolved shear stresses $\tau_\alpha = \mathrm{tr}(\boldsymbol{S}\boldsymbol{C}\boldsymbol{d}_\alpha \otimes \boldsymbol{n}^\alpha)$ and internal variables. The slip rates are assumed to be governed by a power-law expression $\dot{\mu}_\alpha = \dot{\mu}_0\,\mathrm{sign}(\tau_\alpha)|\tau_\alpha/\tau^C_\alpha|^N$.

Hardening: The simulations are limited to constant velocity gradients. Therefore, only isotropic hardening models are taken into account. The internal variables τ^C_α are assumed to be functions of the accumulated shear strains $z^\alpha := \int|\dot{\mu}^\alpha|\,\mathrm{d}t$. Two different hardening models are applied. The first model (IH1) is a modification of that used in Harren et al. [13]:

$$\tau_\alpha^C = \tau_0^C + \sum_{\beta=1}^{12} h_S q_{\alpha\beta} z_\beta + (\tau_S - \tau_0)\ \tanh\left(\frac{h_0 - h_S}{\tau_S - \tau_0^C}\sum_{\beta=1}^{12} q_{\alpha\beta} z_\beta\right). \quad (14)$$

The modification concerns the introduction of cross-effects by $q_{\alpha\beta}$ in the last term. The second model (IH2) is taken from [19]:

$$\tau_\alpha^C = \tau_0^C + \sum_{\beta=1}^{12} H q_{\alpha\beta}(1 - \exp(-B z_\beta)). \quad (15)$$

Material constants: The elastic constants are given by $K_{1111} = 168$ GPa, $K_{1122} = 121$ GPa, $K_{1212} = 75$ GPa. The reference shearing rate is taken as $\dot{\mu}_0 = 1/1000$ s and the inverse of the strain rate sensitivity as $N = 80$. The initial critical shear stress τ_α^C is assumed to be equal for all slip systems and is set to $\tau_0^C = 16$ MPa. The hardening parameters of the first model are taken from [24] with exception of τ_S, which is due to the above mentioned modification of the model. The parameters specifying the second model are chosen such that the polycrystal stress-strain curve given by the first model is obtained. The parameters are given by $\tau_S = 100$ MPa, $h_0 = 132$ MPa, and $h_S = 7.68$ MPa, $H = 10$ MPa, and $B = 15$. The matrix elements $q_{\alpha\beta}$ are equal to 1 for $\alpha = \beta$ and coplanar systems and 1.4 otherwise.

Simulated processes: In this paper the texture induced elastic anisotropy is investigated by simulating a plane strain compression (A), a drawing (B), and a simple shear deformation (C). The corresponding deformation gradients are given by

$$\begin{aligned}
&\text{A}: \quad \boldsymbol{F} = \kappa \boldsymbol{e}_1 \otimes \boldsymbol{e}_1 + \kappa^{-1} \boldsymbol{e}_2 \otimes \boldsymbol{e}_2 + \boldsymbol{e}_3 \otimes \boldsymbol{e}_3, \quad \kappa \in [1, 10],\\
&\text{B}: \quad \boldsymbol{F} = \kappa \boldsymbol{e}_1 \otimes \boldsymbol{e}_1 + \kappa^{-1/2}(\boldsymbol{e}_2 \otimes \boldsymbol{e}_2 + \boldsymbol{e}_3 \otimes \boldsymbol{e}_3), \quad \kappa \in [1, 10],\\
&\text{C}: \quad \boldsymbol{F} = \boldsymbol{I} + \kappa \boldsymbol{e}_1 \otimes \boldsymbol{e}_2, \quad \kappa \in [0, 5].
\end{aligned} \quad (16)$$

In Fig. 1 the norm $D := \|\mathbf{D}\|$ is shown for the simple shear deformation. The curves determined from a calculation with 1000 modified random orientations [7] and the two aforementioned hardening laws indicate that the predictions of both hardening models are almost the same. For shear numbers larger than $F_{12} \approx 5$ the results depend strongly on the parameters in both the flow and hardening rule.

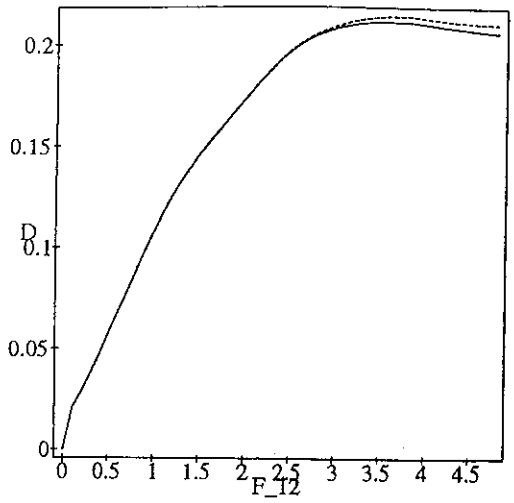

Fig. 1. D vs F_{12} for simple shear ((–): IH1, (- -): IH2).

The norm D is shown in Fig. 2 for the plane strain compression and the drawing deformation. In the former case no saturation of anisotropy is observed in the range $F_{A11} \in [0, 10]$, in the latter the magnitude of $\mathbf{D}$ is stationary in the range $F_{B11} \in [6, 10]$, and so are the components of $\mathbf{K}^V$.

Young's modulus predicted by $\mathbf{K}^V$ due to a plane strain compression deformation with a thickness reduction of 90% as a function of the orientation $\{\varphi, \theta\}$ is plotted in Fig. 3. The angles

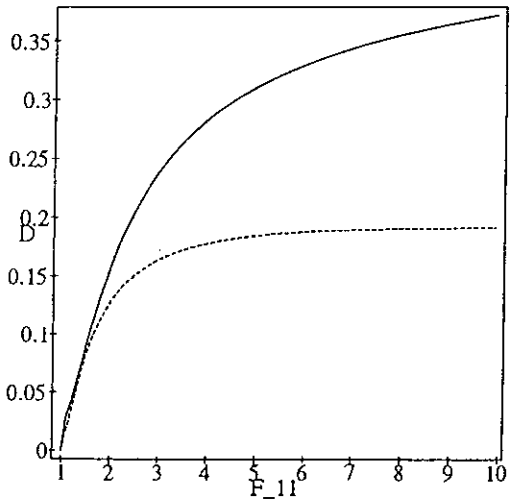

Fig. 2. D vs F_{11} for plane strain compression (–) and uniaxial drawing (- -).

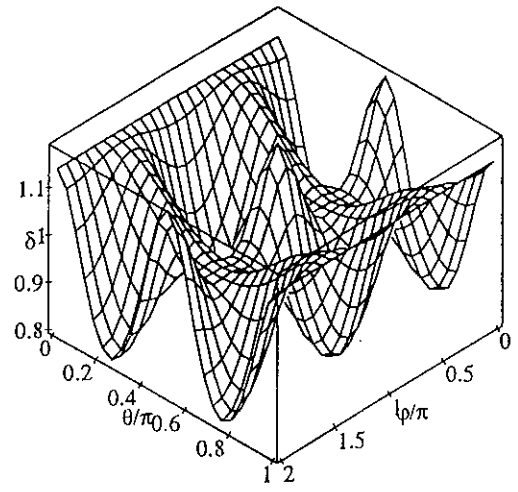

Fig. 3. Young's modulus $\delta = E^{V}/E^{VI}$ for $F_A(\kappa = 10)$.

$\{\varphi = 0, \theta = \pi/2\}$, $\{\varphi = \pi/2, \theta = \pi/2\}$, and $\{\theta = 0\}$ correspond to the rolling (RD), normal (ND), and transverse direction (TD), respectively. The modulus is normalized by the value predicted by the isotropic bound. In rolling and transverse direction the modulus is increased up to 15%. The maximal decrease of 20% occurs in direction $\{\varphi = 0, \theta = \pi/4\}$. In Fig. 4 the modulus is shown as predicted in the sheet plane ($\theta = 0$: TD, $\theta = \pi/2$: RD). This result corresponds to experiments with copper documented in Ref. [17].

Material symmetry: In order to solve the problem $\|\mathbf{K}^{V} - \mathbf{K}^{VA}\| \to \min$ for a given $\mathbf{K}^{V}$, a direct search polytope algorithm [11] has been used. The standard representations of $\mathbf{K}^{VA}$ for different symmetry classes can be easily used, if $\|\Delta\mathbf{K}\|$ is parameterized in form of

$$\|K^{V}_{ijkl} - Q_{im}Q_{jn}Q_{ko}Q_{lp}\bar{K}^{VA}_{mnop}\| \to \min,$$

where $\bar{K}^{VA}_{mnop}$ are the components of $\mathbf{K}^{VA}$ with respect to the symmetry axes of the material. The orthogonal matrix $\boldsymbol{Q}$ is determined by an orientation vector $\boldsymbol{m}$ according to $\boldsymbol{Q} = \exp(\varepsilon\,[\boldsymbol{m}])$, ε being the third-order permutation tensor. The rotation angle and axis are given by $W = |\boldsymbol{m}|$, and $\boldsymbol{n} = \boldsymbol{m}/|\boldsymbol{m}|$, respectively.

In Fig. 5 the norm $A := \|\Delta\mathbf{K}^{*}\|$ with $\Delta\mathbf{K}^{*} := (\mathbf{K}^{V} - \mathbf{K}^{VA})/\|\mathbf{K} - \mathbf{K}^{VI}\|$ is shown for the plane strain compression deformation and approximations $\mathbf{K}^{VA}$ having the following symmetry groups: (–) = isotropy; (- -) = transverse isotropy $\mathscr{C}_{12}$ and hexagonal systems $\mathscr{C}_{10,11}$; □ = hexagonal systems $\mathscr{C}_{8,9}$; (–) = cubic system $\mathscr{C}_{6,7}$; (◇) = tetragonal systems $\mathscr{C}_{4,5}$; (○) = orthotropic system $\mathscr{C}_{3}$; (+) = monoclinic system $\mathscr{C}_{2}$ [12]. The parameter A describes the deviation of the approximation $\mathbf{K}^{VA}$ from the upper bound $\mathbf{K}^{V}$ normalized by the elastic anisotropy of the single crystal. The approximation with an orthotropic symmetry leads to a significant reduction of $\|\Delta\mathbf{K}^{*}\|$, which indicates that $\mathbf{K}^{V}$ possesses an orthotropic symmetry within an acceptable tolerance.

In Fig. 6 the norm A is shown for a drawing deformation. In contrast to the rolling deforma-

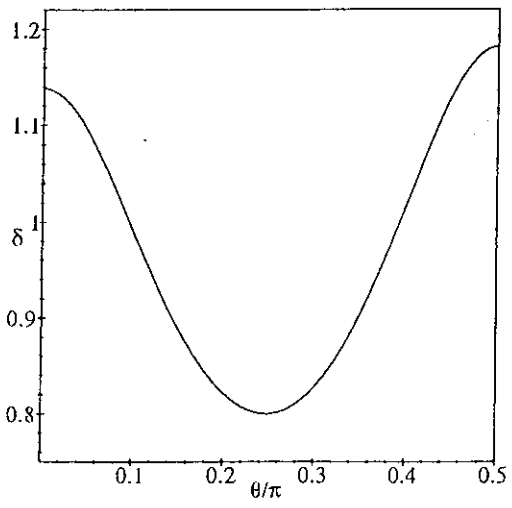

Fig. 4. Young's modulus $\delta = E^{V}/E^{VI}$ for $F_A(\kappa = 10)$ in the sheet plane.

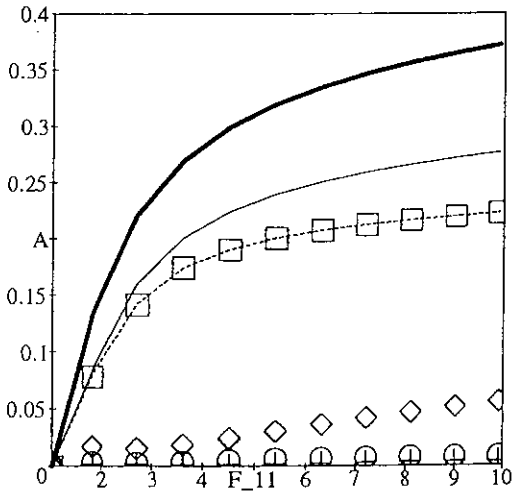

Fig. 5. A vs F_{11} for plane strain compression.

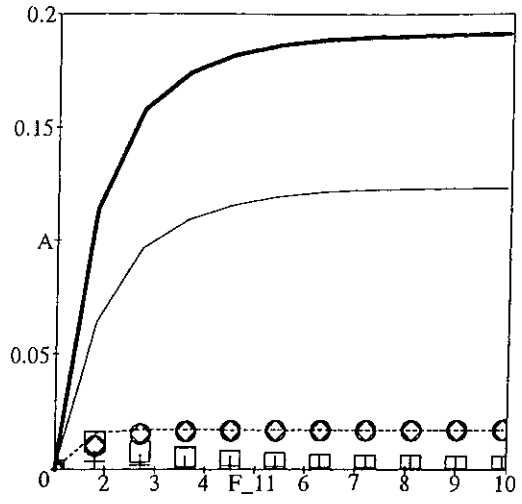

Fig. 6. A vs F_{11} for drawing.

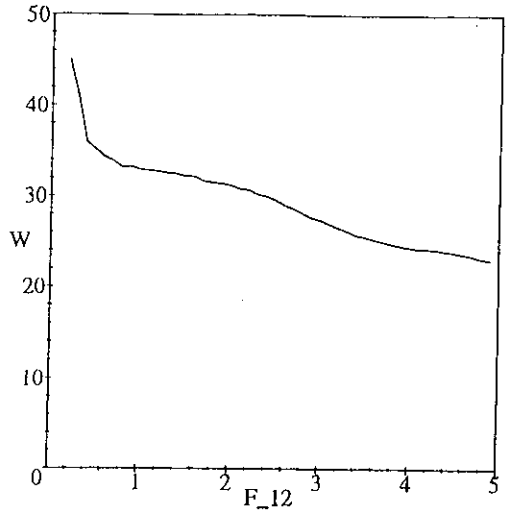

Fig. 8. Rotation angle W (in degrees) vs F_{12} for simple shear.

tion, here the approximation with a hexagonal symmetry ($\mathscr{C}_{8,9}$) yields better results than the one with a rhombic, i.e., orthotropic, symmetry. In Fig. 7, the norm A is plotted corresponding to different symmetry groups for the simple shear mode. In contrast to the aforementioned deformation modes, a rotation of the macroscopic symmetry axes is observed. The vector $\boldsymbol{m}$ has only a non-vanishing component in direction of the mirror plane normal $\boldsymbol{e}_3$. The rotation angle W corresponding to the orthotropic approximation as function of the shear number is shown in Fig. 8.

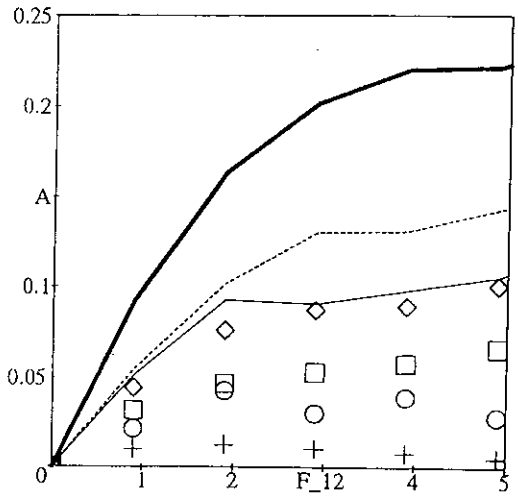

Fig. 7. A vs F_{12} for simple shear.

5. Conclusions

The texture induced anisotropy of the elastic properties of polycrystalline copper is studied for three different proportional deformation modes. The macroscopic elastic properties are determined by volume averages, which give bounds for the stored energy of the real material. These volume averages are generally – similar to real materials – triclinic. In order to obtain information concerning the material symmetry, approximations of the volume averages with different symmetry groups are determined and compared. As a result the history of the macroscopic elasticity tensors can be analyzed with respect to the governing symmetry group and the orientation of the macroscopic symmetry axes.

There are three extensions of the investigation of some interest. (1) Since the Taylor–Lin model is applied, deformation inhomogeneities are excluded during the inelastic process. A finite element simulation would include such heterogeneities and predict textures less sharp and closer to experimental data [6]. Furthermore, this approach allows to investigate the effect of a morphological texture on the macroscopic properties. (2) An introduction of kinematical hardening effects on the slip system level is necessary to analyze cyclic deformation modes. (3) The development of phenomenological evolution laws can be done close to the micro-macro-simulations in order to take into

account the texture evolution which is the main reason for induced elastic and inelastic anisotropy in the case of intermediate and large deformations.

References

[1] K. Aleksandrov, L. Aizenberg, Dokl. Akad. Nauk. SSSR 167 (1967) 1028–1031.

[2] R.J. Asaro, A. Needleman, Texture development and strain hardening in rate dependent polycrystals, Acta Metall. 33 (1985) 923.

[3] A. Bertram, An alternative approach to finite plasticity based on material isomorphisms, Int. J. Plast. 5 (3) (1999) 353–374.

[4] A. Bertram, K. Kraska, Description of finite plastic deformations in single crystals by material isomorphisms, in: D.F. Parker, A.H. England (Eds.), Proceedings of IUTAM Symposium on Anisotropy, Inhomogeneity and Nonlinearity in Solid Mechanics, 30.8.-3.9.1994, Nottingham, 1995, pp. 77–90.

[5] A. Bertram, J. Olschewski, Formulation of anisotropic linear viscoelastic constitutive laws by a projection method, in: A. Freed, K. Walker (Eds.), High Temperature Constitutive Modelling: Theory and Application, ASME, 1991, MD-vol. 26, AMD-vol. 121, pp. 129–137.

[6] A. Bertram, T. Böhlke, M. Kraska, Texture development of aluminum polycrystals under finite plastic deformations, in: O.T. Bruhns, E. Stein (Eds.), Micro- and Macrostructural Aspects of Thermoplasticity, 1998, pp. 127–136.

[7] T. Böhlke, A. Bertram, Simulation of texture development and induced anisotropy of polycrystals, in: S. Alturi, P. O'Donoghue (Eds.), Proceedings of ICES'98, Modeling and Simulation Based Engineering, 1998, pp. 1390–1395.

[8] H. Bunge, Texture Analysis in Material Science, Cuviller Verlag, Göttingen, 1993.

[9] S. Cowin, M. Mehrabadi, On the identification of material symmetry for anisotropic elastic materials, Q. J. Mech. Appl. Math. 40 (1987) 451–476.

[10] N. Gaffke, B. Heiligers, Priv. Communic, Institute of Mathematical Stochastic, University Magdeburg, 1998.

[11] P.E. Gill, W. Murray, M. Wright, Practical Optimization, Academic Press, New York, 1981.

[12] M.E. Gurtin, The Linear Theory of Elasticity, Encyclopedia of Physics, vol. VIa/2, Springer, Berlin, 1972.

[13] S. Harren, T. Lowe, R. Asaro, A. Needleman, Analysis of large-strain shear in rate-dependent face-centered cubic polycrystals: Correlation of micro- and macro-mechanics, Phil. Trans. R. Soc. Lond. A 328 (1989) 443–500.

[14] R. Hill, The elastic behaviour of a crystalline aggregate, Proc. Phys. Soc. Lond. A 65 (1952) 349–354.

[15] U. Kocks, C. Tome, H. Wenk, Texture and Anisotropy: Preferred Orientations in Polycrystals and Their Effect on Materials Properties, Cambridge University Press, Cambridge, 1998.

[16] T. Leffers, Microstructures, textures and deformation patterns at large strains, in: S. Teodosiu Raphanel (Ed.), MECAMAT'91, ISBN 9-05-410317-5, 1993, pp. 73–86.

[17] Y. Liu, G. Alers, The anisotropy of Young's modulus in cold rolled sheets of binary Cu–Zn alloys, Trans. AIME 236 (1966) 489–495.

[18] S. Matthies, M. Humbert, On the principle of a geometric mean of even-rank symmetric tensors for textured polycrystals, J. Appl. Cryst. 28 (1995) 254–266.

[19] L. Méric, G. Cailletaud, M. Gaspérini, Calculations of copper bicrystal specimens submitted to tension–compression tests, Acta Metall. Mater. 42 (3) (1994) 921–935.

[20] S. Nemat-Nasser, M. Hori, Micromechanics: Overall Properties of Heterogeneous Materials, Elsevier, Amsterdam, 1993.

[21] A. Reuss, Berechnung der Fließgrenze von Mischkristallen auf Grund der Plastizitätsbedingung für Einkristalle, Angew. Math. Mech. 9 (1929) 49–58.

[22] W. Voigt, Lehrbuch der Kristallphysik, Leipzig, Teubner, 1928.

[23] G. Wasserman, J. Grewen, Texturen metallischer Werkstoffe, Springer, Berlin, 1962.

[24] P. Wu, K. Neale, E. Van der Giessen, Simulation of the behaviour of fcc polycrystals during reversed torsion, Int. J. Plast. 12 (9) (1996) 1199–1219.